Polarized-beam study of the paramagnetic scattering from bcc iron

J. P. Wicksted, P. Böni, and G. Shirane
Brookhaven National Laboratory, Upton, New York 11973
(Received 20 April 1984)

Reliable magnetic scattering cross sections are obtained for bcc Fe at $T=1.02T_c$ and $1.06T_c$ using polarized neutrons and polarization analysis. The constant-q measurements cover a q range of 0.1–0.6 Å^{-1} with an energy range extending up to 50 meV. These scans consist of broad energy distributions centered at zero energy with no peaks observed at finite-energy transfers, in contrast to the results reported by Lynn. A simple paramagnetic scattering function $S(q,\omega)\propto[1/(\kappa_1^2+q^2)][\Gamma/(\Gamma^2+\omega^2)]$ is shown to describe the iron cross sections quantitatively, and in absolute units, for the q and energy range specified above. The peaks observed in constant-energy scans are simply energy slices of the paramagnetic scattering function and thus should not be interpreted as spin-wave peaks. We conclude that in the (q,ω) region covered in our polarized beam studies, neither propagating spin waves nor giant short-range magnetic order exist in Fe above T_c.

I. INTRODUCTION

The spin correlations in the paramagnetic state of iron have been the center of much controversy for the past decade.[1] Early inelastic neutron investigations conducted at Brookhaven by Collins *et al.*[2] on Fe showed that for small momentum transfers, spin waves just below the Curie temperature (T_c) continuously changed to critically damped modes at temperatures slightly above T_c. Several years later, Lynn[3] conducted constant-energy neutron-scattering experiments on Fe, reporting the existence of a persistent spin-wave dispersion above T_c at energy values exceeding 8 meV. Lynn also reported one constant-q scan at 0.47 Å^{-1} which showed a spin-wave-like peak. A similar conclusion was also obtained for Ni by Mook *et al.*[4] and Lynn and Mook[5] using constant-energy scans; however, no constant-q scans have been reported.

Local band theories[6] were subsequently developed which required a giant short-range magnetic order (SRMO) to explain Lynn's results. A more conventional effective Heisenberg model[7] was also developed which could qualitatively reproduce the constant-energy peaks observed in Fe, but could not explain the published constant-q data at $q=0.47$ Å^{-1}. More recently, Brown *et al.*,[8] at Institut Laue-Langevin (ILL), Grenoble, have reported paramagnetic scattering measurements in several $3d$ transition metals utilizing polarized neutrons and polarization analysis. Brown *et al.*[8] intentionally used a large energy resolution [full width at half maximum (FWHM) $\approx$43 meV] to conduct their experiments. They have interpreted their results in Fe (Refs. 9 and 10) as being in agreement with the local band theories and have concluded that ferromagnetic correlations of up to 15 Å exist for temperatures well above T_c. However, Edwards[11] has subsequently reanalyzed the Fe results obtained by Brown *et al.*[9] at $T=1.25T_c$ and claims that a much smaller SRMO is present in the paramagnetic phase.

Recently, a series of neutron-scattering experiments[12–15] have been conducted at Brookhaven National Laboratory on Fe and Ni in an attempt to properly characterize the paramagnetic scattering and thus help resolve the issue on the size of the SRMO in the paramagnetic phases of these two classical ferromagnets. Steinsvoll *et al.*[12,13] have utilized polarized- and unpolarized-neutron studies performed with sufficient energy and q resolution to properly characterize the magnetic scattering function $S(q,\omega)$ of Ni over the q region 0.14 to 0.4 Å^{-1}. The constant-energy scans conducted in these experiments showed results very similar to those obtained by Lynn and Mook,[5] however, no corresponding spin-wave peaks were observed in constant-q scans over the q and energy ranges covered. Instead, broad energy distributions of Lorentzian-type line shapes centered at zero energy transfer were observed. Polarized-beam studies were also performed on Fe–4 at.% Si by Wicksted, Shirane, and Steinsvoll.[14,15] The constant-q scans also showed Lorentzian-type behavior for the magnetic scattering over a range of q from 0.12 to 0.5 Å^{-1}. In particular, no constant-q spin-wave peaks were observed, in contrast to the constant-q scans published by Lynn.[3,16] The energy integration of these constant-q results were in reasonably good agreement with those obtained by Brown *et al.*[9] The importance of using polarized neutrons and polarization analysis has also been pointed out from these Fe experiments, since both single and multiphonon scattering processes can distort the paramagnetic scattering when using unpolarized neutrons with large energies. These polarized-beam studies conducted at Brookhaven on Fe and Ni have resulted in an entirely new interpretation of the paramagnetic scattering. Neither propagating spin waves nor spin-wave dispersion curves exist above T_c for the q and energy ranges covered. Instead, the following simple scattering function has been shown to qualitatively describe the paramagnetic scattering for Fe and Ni:

$$S(q,\omega)\propto\frac{1}{\kappa_1^2+q^2}\frac{\Gamma}{\Gamma^2+\omega^2}\ . \tag{1}$$

Although this double-Lorentzian form of the scattering

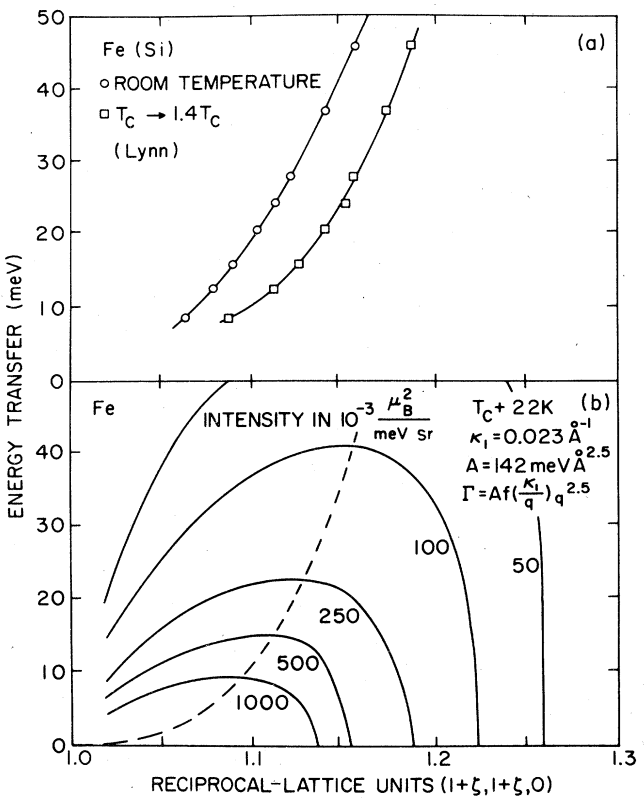

FIG. 1. (a) "Spin-wave" dispersion curves obtained from Ref. 3 (Fig. 2) for Fe at room temperature and for $T \geq T_c$. (b) Intensity contours calculated from Eq. (2) using Fe parameters from Table II.

function is quite general, the values of the inverse correlation length κ_1 and linewidth Γ used in the comparison with the neutron experiments have been scaled from the values obtained in the critical paramagnetic studies of Fe and Ni.[2,17] The constant-energy peaks observed in the neutron measurements can now be interpreted as energy slices of the paramagnetic scattering which results from Eq. (1). Lynn and Mook had originally concluded that these constant-energy peaks represented spin waves resulting in the spin-wave dispersion curve given in Fig. 1(a) (see Ref. 3). Their interpretation was based on the conversion of $\Delta q/q \rightarrow \Delta E/E$ with the condition $\Delta E/E < 1$. Such a conversion is not a justifiable one, as can be seen from the intensity contours of Fig. 1(b), which are obtained from Eq. (1). Earlier we were convinced that Eq. (1) could correctly explain the constant-energy peaks for energies up to 40 meV; however, we still believed that at higher energies these peaks represented "spin waves."

Recently, however, Uemura *et al.*[18] carried out a model calculation on Ni and concluded that Eq. (1) can explain the constant-energy ridges observed by Lynn and Mook[5] up to 80 meV. It was further suggested that this simple paramagnetic scattering function could be applied to the paramagnetic phases of EuO and MnSi. At T_c, Shirane *et al.*[19] demonstrated that Eq. (1) reduces to a universal form which, when properly scaled, can describe the paramagnetic scattering from all isotropic cubic ferromagnets

In this paper new polarized-neutron-scattering results are reported from pure Fe above T_c for a q range 0.1 to 0.6 Å^{-1}. In particular, the present $S(q,\omega)$ data and its energy integration [denoted by $M^2(Q)$] obtained from the pure-Fe crystal are quantitatively compared with the simple paramagnetic scattering function, convoluted with the instrumental resolution using parameters scaled from the values originally obtained by Collins *et al.*[2] In Sec. II the experimental configurations used for the polarized- and unpolarized-neutron-scattering studies are described along with the technique of transforming the data into absolute intensity units. In Sec. III the properties of the paramagnetic scattering function are described while in Secs. IV and V we present the results along with the detailed analysis performed on the Fe data. In Sec. VI we discuss the implication of these results in addition to answering some of the questions which have recently been raised regarding the validity of the simple paramagnetic sattering formula.

II. POLARIZED-BEAM TECHNIQUE

All neutron-scattering experiments were performed at the Brookhaven High Flux Beam Reactor. The iron crystal is cylindrical in shape, with a diameter of 8 mm and a length of 30 mm. The [1$\bar{1}$0] crystal axis is along the cylinder axis and mounted vertically. Polarized triple-axis scans are conducted in the [110] direction in the neighborhood of the (1,1,0) reciprocal-lattice point. The reciprocal-lattice spacing is $\approx$3.06 Å^{-1} when the sample is at its Curie temperature T_c ($\approx$1043 K). Only two temperatures above T_c are studied (1.02T_c and 1.06T_c). The temperature of the Fe sample, however, never approached the γ-phase value (1183 K) where the crystal structure becomes fcc.

For the polarization analysis of the iron crystal, vertically magnetized Heusler (111) transmission crystals are used as monochromators and analyzers, with magnetic guide fields which maintain the polarization of the neutrons [see Fig. 2(a)]. These scattering experiments are conducted with final fixed energies of 14.7, 30.5, and 60 meV, and with collimations of 40′-40′-40′-40′ or 40′-80′-80′-80′. Table I summarizes the energy and q resolutions which result from these instrumental conditions. A flat-coil spin flipper is used and the overall instrumental flipping ratio is between 12 and 18. Most of the earlier polarized-beam experiments were performed with an external 120-Oe magnetic guide field imposed at the sample along the horizontal scattering vector. However, recent polarized-beam experiments conducted on the pure-Fe sample utilized magnetic fields at the sample which are parallel (horizontal) and perpendicular (vertical) to the horizontal scattering vector. This technique of subtracting data obtained in the vertical-field configuration from that in the horizontal-field configuration eliminates both background and nuclear scattering contributions.[20]

The majority of the polarized-beam experiments are performed above T_c in order to directly study the

TABLE I. Wave vector (ΔQ) and energy resolutions (ΔE) at specific Q values and energy transfers.

	Q	E_i	E_F	Collimation	$\Delta Q[110]$	$\Delta Q[1\bar{1}0]$	ΔE
$1+\zeta$	(Å^{-1})	(meV)	(meV)	(min)	(Å^{-1})	(Å^{-1})	(meV)
1.10	3.36	41	30.5	40-80-80-80	0.07	0.16	5.68
1.15	3.51	80	60.0	40-40-40-40	0.12	0.22	10.60
1.10	3.36	70.5	60.0	40-80-80-80	0.10	0.21	14.20

paramagnetic scattering from the two iron samples. However, some experiments on pure Fe are performed below T_c, where the sample, in its ferromagnetic state, now depolarizes the neutron beam. For these experiments, the flipper and all external fields at the sample are turned off since no polarization analysis is possible. The reason for these "unpolarized" measurements is to verify that the resolution used in our polarized-beam experiments above T_c is indeed sufficient to show if propagating spin waves are present or not. An example of the unpolarized investigation conducted on pure Fe is given in Fig. 3(a) at (1.12,1.12,0) ($q=0.367$ Å^{-1}) and T_c-332 K. Included in this figure is nuclear scattering from the LA and TA phonons, the latter effect resulting from the vertical instrumental resolution. The magnon centered at 22.5 meV is clearly visible in this constant-q scan. This shows that the resolution used in our polarized-beam investigations is sufficient in determining whether constant-q spin-wave peaks are present or not for temperatures above T_c.

The power of polarized neutrons and polarization analysis is clearly illustrated in Figs. 3(b) and 3(c). In Fig. 3(b) a constant-q scan at (1.1,1.1,0) ($q=0.31$ Å^{-1}) obtained from the Fe sample via polarization analysis at $T=T_c+22$ K is shown. The open circles represent data obtained with the flipper "on" and the magnetic field in the direction of the horizontal scattering vector. In this configuration, the data consists of the paramagnetic

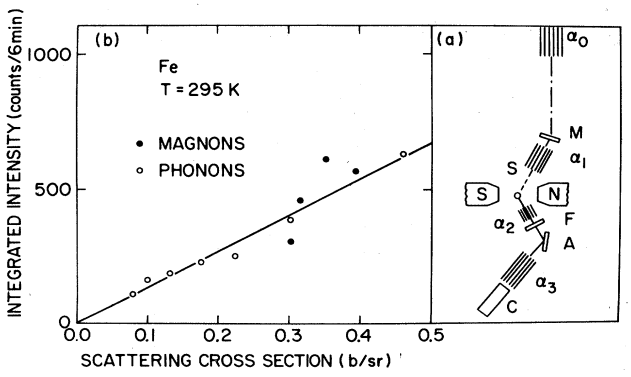

FIG. 2. (a) Schematic diagram of the triple-axis spectrometer used in our polarized-beam investigations. (b) Calibration curve resulting from phonon and magnon measurements from Fe at room temperature.

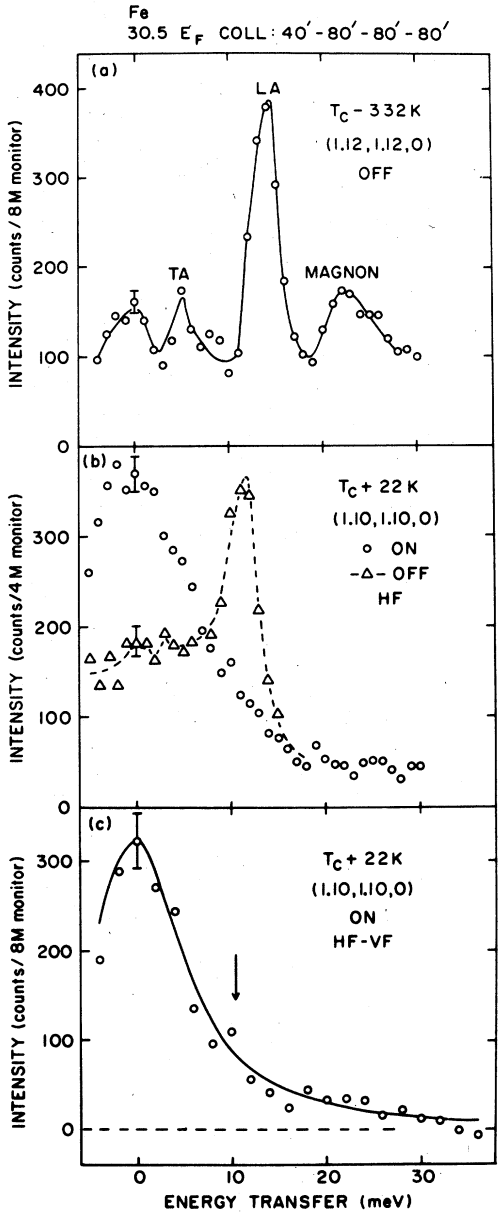

FIG. 3. (a) "Unpolarized"-neutron study of Fe at (1.12,1.12,0) and $T\approx T_c-332$ K. Both flipper and external magnetic field are "off." (b) Polarized-beam study at (1.10,1.10,0) and $T=1.02T_c$ with horizontal magnetic field at sample. Open circles denote data obtained with flipper "on," while open triangles and dashed curve illustrate data obtained with flipper "off." (c) Polarized-beam study at (1.10,1.10,0) and $T=1.02T_c$ with horizontal—vertical magnetic field difference of flipper "on" data. Solid line in (c) results from Eq. (2). M in ordinate label denotes the numerical value of 10^6.

scattering. Also shown is the nuclear scattering, which is represented by the open triangles and obtained with the flipper "off". The separation between the nuclear and magnetic scattering is seen very clearly in this figure, although it should be noted that the "on" data does contain additional contributions due to background effects, nuclear-spin incoherent scattering, and some contamination from the "off" intensity due to the finite value of the flipping ratio. The open circles in Fig. 3(c), which were obtained at the same q as in Fig. 3(b) with the flipper on, result through the subtraction of the data with the magnetic field perpendicular (vertical field) to the scattering vector at the sample from the data with the field parallel (horizontal field) to the scattering vector. The data obtained with the vertical magnetic field consist of one-half of the paramagnetic scattering and the additional contributions mentioned above. Therefore, the vertical-field (VF) subtraction from the horizontal field (HF), with the flipper on, results in data which are purely magnetic (one-half paramagnetic scattering) and which can be directly compared to the convolution of Eq. (1) with the instrumental resolution function (solid line).

The difference technique (HF−VF) is essential when the magnetic cross section becomes smaller than the instrumental background; for example, the high-energy data of Fig. 3(b). The counting time in constant-q scans with E_F fixed changes considerably as a function of energy transfer; thus a reliable estimate of the background for the "on" data becomes impossible at high-energy transfers. These difficulties are completely eliminated in the difference data of Fig. 3(c).

Experiments were performed on the Fe crystal such that phonon cross sections both above and below T_c (and magnons below T_c) were measured. The calculation of the theoretical cross sections for magnons and phonons, in conjunction with the measured cross sections, establishes an absolute intensity scale. This technique calibrates the triple-axis spectrometer such that for a fixed set of conditions (collimation, final fixed energy), the counts per meV obtained from the paramagnetic scattering via a constant-q scan can be converted into barns per meV or μ_B^2 per meV per unit solid angle. This enables direct comparisons to various theories which have calculated the magnetic scattering function $S(q,\omega)$ for the paramagnetic phase of several transition metals. Figure 2(b) shows the results of this calibration for the pure-Fe sample obtained using unpolarized neutrons at room temperature.

III. PARAMAGNETIC SCATTERING FUNCTION

The general form of the magnetic scattering cross section is

$$\frac{d^2\sigma}{d\omega\, d\Omega}=\gamma_0^2 f^2(Q)e^{-2W}S(q,\omega)\ ,$$

where γ_0^2 has the value of 0.291 barns, $f(Q)$ is the magnetic form factor, and e^{-2W} is the Debye-Waller factor.

The early Brookhaven investigations[2] showed that, for small momentum transfers in the critical regions of Fe and Ni, a simple double-Lorentzian scattering function[21] could be used to explain the magnetic scattering

$$S(q,\omega)=\frac{2}{3}\frac{S(S+1)}{r_1^2}\frac{1}{\kappa_1^2+q^2}\frac{1}{\pi}\frac{\Gamma}{\Gamma^2+\omega^2}\frac{\omega/kT}{1-e^{-\omega/kT}}\ . \tag{2}$$

Here, r_1 is the interaction distance, κ_1 is the inverse correlation length, and Γ is the half width at half maximum (HWHM). Equation (2) is a very general paramagnetic scattering function which, in the critical region, utilizes the following expressions for κ_1 and Γ:

$$\kappa_1=\kappa_0\left[\frac{T-T_c}{T_c}\right]^{0.7}\ , \tag{3}$$

$$\Gamma=Aq^{5/2}f(\kappa_1/q)\ . \tag{4}$$

The Résibois-Piette function[22] $f(\kappa_1/q)$ is unity at T_c and becomes proportional to $(\kappa_1/q)^{1/2}$ in the hydrodynamic region. The existence of this function in the critical region of Fe has been well established by previous neutron-scattering investigations.[2,23–25] For fixed energy ω, Eq. (2) has a maximum value at finite q, while for fixed q the function peaks at zero energy (although a broad peak at finite energy may result when the detailed balance factor is not close to unity). These features of $S(q,\omega)$ qualitatively agree with the constant-energy neutron scans observed by Mook *et al.*[4] and Lynn and Mook,[5] as well as the constant-q scans reported by Steinsvoll *et al.*[12,13] in Ni. At the Curie temperature, T_c, Eq. (2) can be expressed as

$$S(q,\omega/A)=\frac{S_0}{A}\frac{q^{1/2}}{q^5+(\omega/A)^2}\ , \tag{5}$$

with

$$S_0\equiv 2S(S+1)/(3\pi r_1^2)\ .$$

This form of the scattering function at T_c can be universally applied to all isotropic cubic ferromagnets provided the energy is scaled by A. The general scattering function given by Eq. (2) can also be written as follows:

$$S(q,\omega)=\tfrac{2}{3}S(S+1)\frac{\chi(0)}{\chi_1}\frac{\kappa_1^2}{\kappa_1^2+q^2}\frac{1}{\pi}\frac{\Gamma}{\Gamma^2+\omega^2}\frac{\omega/kT}{1-e^{-\omega/kT}}\ . \tag{6}$$

The parameters κ_1 and r_1 have been related to the static susceptibility $\chi(0)$ via the expression

$$\frac{1}{(r_1\kappa_1)^2}=\frac{\chi(0)}{\chi_1}\ , \tag{7}$$

where χ_1 is the susceptibility of a system of noninteracting spins.

The energy integration of Eq. (6), defined as

$$M^2(Q)=6\int S(q,\omega)d\omega\ ,$$

has the form

$$M^2(Q)=\frac{M^2(0)\kappa_1^2}{\kappa_1^2+q^2}\ , \tag{8}$$

TABLE II. Physical properties of iron.

Expression	Quantity	Å^{-1}	Theta units[a]	Temperature
$\kappa_1=\kappa_0[(T-T_c)/T_c]^{0.7}$	κ_0 (Å^{-1})	1.05	0.34	
$T_c=1043$ K	κ_1 (Å^{-1})	0.07	0.023	$1.02T_c$
		0.152	0.05	$1.06T_c$
$\Gamma=Af(\kappa_1/q)q^{2.5}$	A (meV $\text{Å}^{2.5}$)	142.3	2407	
$E=Dq^2$	D (meV Å^2)	320	2996	0
		175	1638	$0.8T_c$

[a]Theta units are given in units of $\text{Å}^{-1}/d^*(110)$ where $d^*(110)=3.06$ Å^{-1}.

where

$$M^2(0)=4S(S+1)\frac{\chi(0)}{\chi_1}\ , \tag{9}$$

and the detailed balance factor has been neglected. The expressions for both $M^2(0)$ and $M^2(Q)$ are in units of μ_B^2. Some of the relevant Fe parameters used in this analysis are given in Table II.

IV. MAGNETIC SCATTERING ABOVE T_c

The paramagnetic scattering results on pure Fe are described in this section. The data, which includes both energy-resolved and energy-integrated results, as well as linewidth measurements, are compared with the theoretical expressions given in Sec. III. The data in Fig. 4 have been obtained in the same manner as in Fig. 3(c), with the flipper on and in the HF—VF configuration. Here, however, the Heusler analyzer is fixed at 60 meV. The three constant-q scans shown at $T=1.02T_c$ have been compared to the theoretical scattering function given by Eq. (2) convoluted with the instrumental resolution. The values of κ_1 and A are given in Table II and were fixed during the analysis. The resolution-convoluted theoretical scattering function in Fig. 4(b) (solid line) was normalized near the data value at zero-energy transfer. The dashed line in Fig. 4(b) represents the scattering function which has been normalized but not convoluted with the resolution function. The normalization values used for the solid lines in Figs. 4(a) [(1.05,1.05,0)] and 4(c) [(1.15,1.15,0)] have been scaled from the value used in 4(b) [(1.10,1.10,0)] via the ratio of the atomic form factors and Debye-Waller factors. Remarkably good agreement is seen between these three constant-q measurements and the theoretical scattering cross section given by Eq. (2).

The arrows in Figs. 4(b) and 4(c) indicate the energy positions where propagating "spin waves" should occur. These peak values were obtained from the spin-wave dispersion curve given by Fig. 2 in Ref. 3. The data are strongly peaked at zero energy transfer for $\zeta<0.1$; however, for larger ζ values, the scattering becomes less enhanced at zero energy and much broader. The

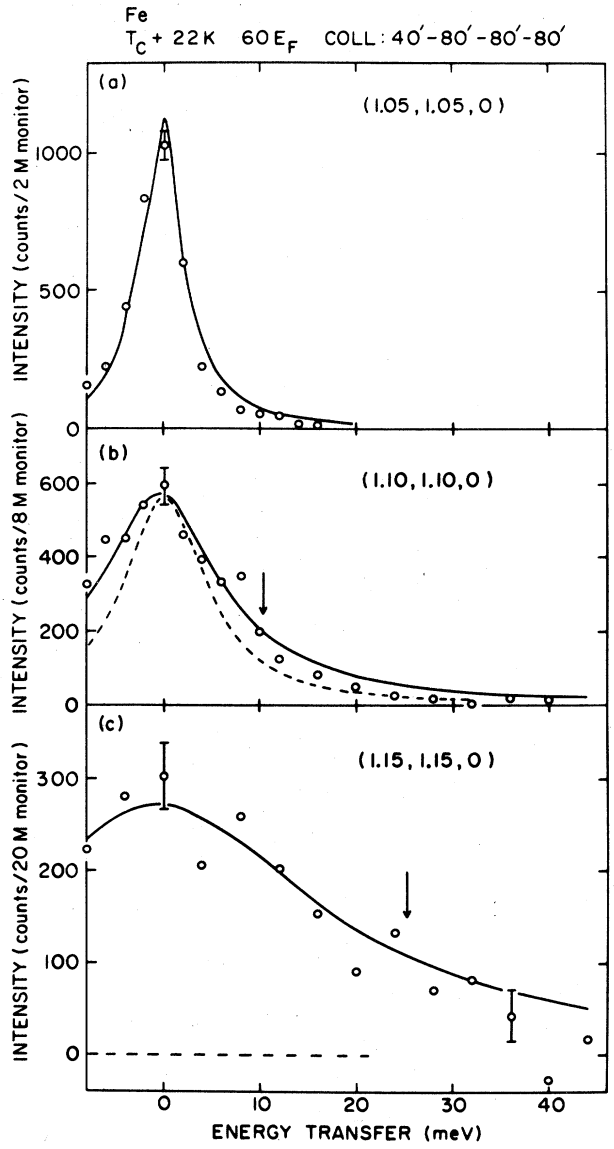

FIG. 4. Paramagnetic scattering data obtained using horizontal—vertical difference technique at $T=1.02T_c$ with (a) (1.05,1.05,0), (b) (1.10,1.10,0), and (c) (1.15,1.15,0). Solid curves in each figure are calculations using Eq. (2). Dashed curve in (b) represents the normalized form of Eq. (2) without convolution of resolution function. Arrows in (b) and (c) point towards expected spin-wave peaks.

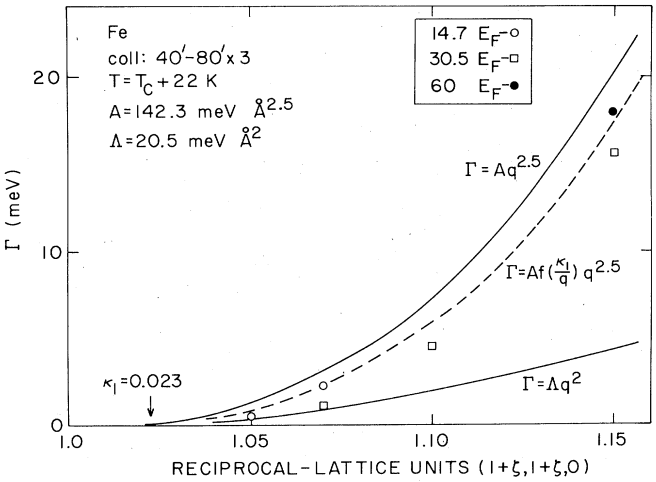

FIG. 5. Linewidth measurements, deconvoluted from the instrumental resolution, as a function of q at $T=1.02T_c$. Three theoretical forms of Γ are shown. Data are obtained using three fixed values of the Heusler analyzer.

Lorentzian behavior of the constant-q scans is quite clear up to $q\approx 0.6$ Å^{-1}. For higher q values the statistics become much poorer, requiring longer counting times. These energy-resolved scans are therefore not as reliable as those constant-q scans with $q<0.6$ Å^{-1}. We have, however, performed constant-q measurements near the zone boundary (~ 1.4 Å^{-1}) using very coarse energy steps. These data yield intensity values (in units of μ_B^2 per meV) which are accurate to about 50%. The behavior of these constant-q scans is quite similar to what we have previously reported from the Fe—4 at. % Si sample.[14,15] Some new measurements concerning this sample are given in Sec. V.

The polarized-beam results were also compared with the theory of Shastry *et al.*[7] This theory had originally been shown to yield constant-E peaks similar to the experimental peaks observed on Ni and Fe.[3–5] This theory also showed constant-q results centered at zero energy which are similar to the experimental data of both Brown *et al.* and our recent results. However, the linewidths of these theoretical results are much narrower than our experimental linewidths, which are given in Fig. 5. For example, at $\zeta=0.05$ the theoretical linewidth is 0.2 meV, while the experimental measurement yields 1.5 meV. These linewidths are resolution-corrected and compiled from three different fixed analyzer-energy values, 14.7, 30.5, and 60 meV, and resulting in FWHM energy resolutions of 1.7, 4.6, and 12 meV, respectively. Three different theoretical forms for Γ as a function of q are illustrated. The observed linewidths agree best with the expression $\Gamma=Aq^{5/2}f(\kappa_1/q)$, which incorporates the Résibois-Piette function. The necessity of the Résibois-Piette function was noted in the previous constant-q investigations of paramagnetic Fe;[22–25] however, the Q range covered in these earlier measurements is below the range covered in our investigation.

The energy integration $M^2(Q)$ for each constant-q scan obtained under the instrumental conditions $30.5E_F$ and $60E_F$ are given in Fig. 6 for $T=T_c+22$ K. The data, denoted by $M^2(Q)$, were first put onto an absolute scale in units of barns by using the calibration technique discussed in Sec. II. The data were then converted into Bohr-magneton-squared units (μ_B^2) using the conversion

$$M^2(Q)=\frac{S(q)}{0.0485f^2(Q)e^{-2W(Q)}}\ , \tag{10}$$

where $S(q)$ is the energy integration, in barns, of the constant-q measurements. These experimental values can then be compared with the theoretical expression for $M^2(Q)$ given in Eq. (8) and represented in Fig. 6 by the solid curve. The value of $M^2(Q)$ at $\zeta=0$ ($\sim 1425\mu_B^2$) has been calculated from the susceptibility [see Eq. (9)]. The agreement between theory and experiment is quite good for $\zeta<0.15$. The inset of Fig. 6 shows an enlarged view of $M^2(Q)$ versus $1+\zeta$ for $\zeta\geq 0.15$. The data in this inset must be regarded as preliminary since they are quite difficult to obtain. The magnetic scattering intensity measurements for these large q values are quite small, requiring long counting times and large energy steps. Each data point corresponds to an effective energy integration from -50 to 50 meV, with an error of $\sim 50\%$. The dotted-dashed curve in the inset corresponds to $M^2(Q)$ in the q region, where this theoretical form [Eq. (8)] is not expected to be valid since higher-order terms in q^2 are expected to become important in the denominator of Eq. (8). The dashed horizontal line in the inset is the wave-vector-independent response expected for an ideal paramagnet with the value of the effective magnetic moment $\mu_{\rm eff}$ ($\approx 3.2\mu_B$) calculated from the Curie constant.

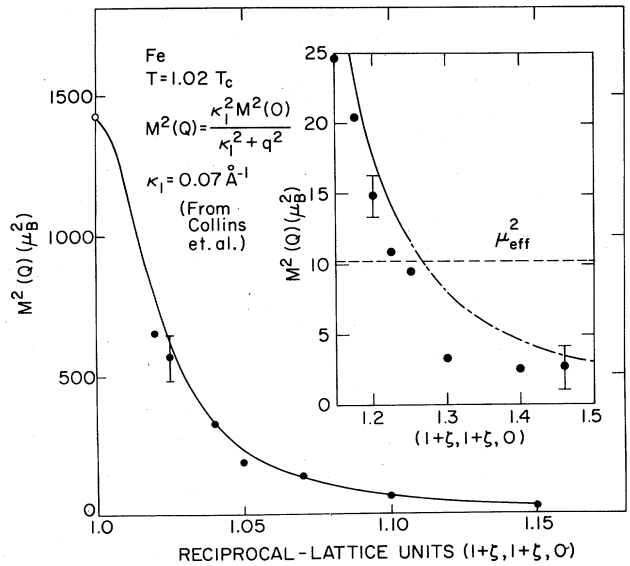

FIG. 6. Energy-integrated paramagnetic scattering $M^2(Q)$ from pure Fe at $T=1.02T_c$. The solid curve results from Eq. (8) with $M^2(0)=1425\mu_B^2$. The inset shows $M^2(Q)$ values extending to the zone boundary. The dashed horizontal line represents ideal paramagnetic scattering with $\mu_{\rm eff}=3.2\mu_B$.

The theoretical q dependence of $M^2(Q)$ is somewhat higher than our data in Fig. 6, especially at large q values where the magnetic intensity is not completely measured due to instrumental limitations. Our interpretation of the data is different from that of the Brown *et al.*[9,10] They have interpreted the missing intensity of their $M^2(Q)$ data at large q values as evidence for giant short-range magnetic order above the Curie temperature in Fe. They estimate the extent of SRMO by calculating $Q^2M^2(Q)$, which yields a peak near $q \approx 0.4$ Å^{-1}, and obtain a correlation length of ≈ 15 Å. We would also obtain such a peak from both our pure-Fe and Fe—4 at. % Si data if we performed this $Q^2M^2(Q)$ calculation; however, we believe that this peak results from the intensity missed by our instrument for $q > 0.4$ Å^{-1}. Note that our $M^2(Q)$ values are consistent for measurements obtained near either the (0,0,0) or (1,1,0) reciprocal-lattice points. Also note that both the large- and small-q energy-integrated data in Fig. 6 yield $M^2(Q)$ values which are approximately 2.5 times larger than the $M^2(Q)$ results obtained earlier by us on Fe—4 at. % Si, and by Brown *et al.* from Fe—5 at. % Si,[9] as well as from the pure-Fe powder.[10]

V. MAGNETIC SCATTERING RESULTS ABOVE AND BELOW T_c—Fe(Si)

Examples of polarized-beam results from the Fe—4 at. % Si sample for temperatures exceeding T_c have been given in two previous reports.[14,15] The magnetic scattering obtained via constant-q scans show broad Lorentzian-type distributions centered at zero energy transfer with no indication of spin-wave-like peaks in the q range covered (0.12—0.5 Å^{-1}). We now illustrate, from this sample, some of the additional unpolarized work which has been performed. Figure 7(a) shows data which contain a magnon peak for a constant-q scan of (0,1.1,1.1) at room temperature. The solid line through this magnon peak is a fit using the spin-wave formula, which holds in a ferromagnet, convoluted with the instrumental resolution,

$$\frac{d^2\sigma}{d\omega\, d\Omega} \propto \frac{k_f}{k_i}\left[\frac{1}{1-\exp(-\omega/kT)}\right]F(Q,\omega)\,, \tag{11}$$

with

$$F(Q,\omega)=\frac{1}{2}\left[\frac{\Gamma}{(Dq^2-\omega)^2+\Gamma^2}\right], \tag{12}$$

where D is the spin-wave-stiffness constant and Γ is the half width at half maximum. Here, $\Gamma=\Lambda q^2$, where Λ, D, and a normalization parameter vary during the fitting procedure. In Fig. 7(b) measurements recorded at T_c-240 K (solid line) and T_c+60 K (dashed line) are given at (0,1.05,1.05) with $T_c \simeq 1031$ K. The data were obtained using a Heusler monochromator and a pyrolytic-graphite analyzer. The magnon is quite apparent at the lower temperature; however, above T_c the bulk of the magnetic scattering is now centered at zero energy transfer, as seen in the previous polarized-beam measurements.

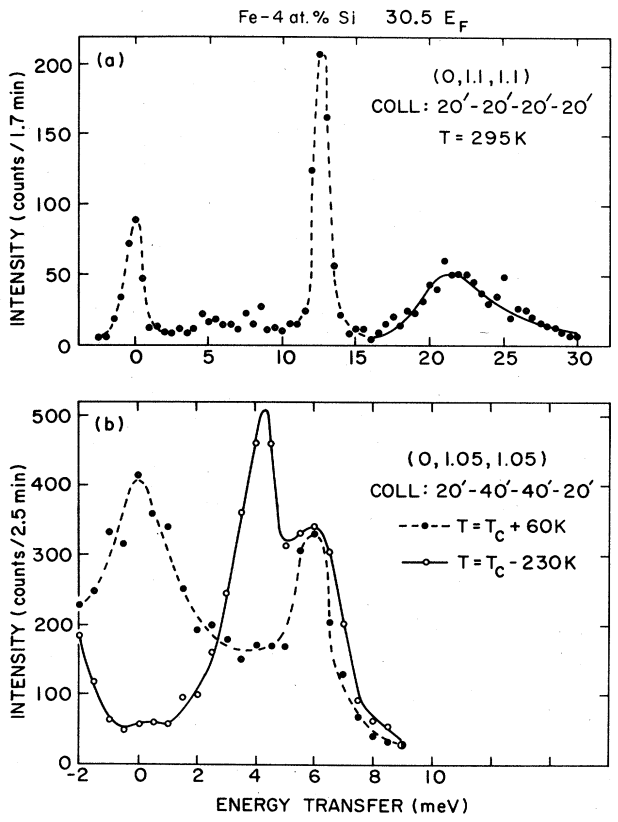

FIG. 7. Constant-q scans performed on Fe—4 at. % Si for (a) (0,1.1,1.1) at room temperature, (b) (0,1.05,1.05) at T_c-230 K (solid curve), and T_c+60 K (dashed curve). All lines in (b) are guides to the eye. The solid curve in (a) represents a fit to the spin-wave data using Eqs. (11) and (12).

We have already demonstrated that our constant-q data, resolution-convoluted, can be described appropriately by a double-Lorentzian form of $S(q,\omega)$, as illustrated in Figs. 3—6. These results should be compared with the data in Fig. 8. The recent paper by Lynn[16] reported that the constant-q data [Fig. 8(a)] published in 1975 was actually arrived at by removing a large background. Figure 8(b) demonstrates this process for a different q value. In the same figure we have quoted two recent constant-q scans reported by Brown *et al.*[9] for similar q values [Figs. 8(c) and 8(d)]. They are essentially in agreement with our data, although they were obtained using a considerably poorer resolution. We should point out that the peak of the data in Fig. 8(b) appears around 20 meV; the "magnon dispersion curve" above T_c previously given shows the peak around ≈ 50 meV for this value of q. We therefore conclude these peaks in Figs. 8(a) and 8(b) are spurious due to an improper background subtraction.

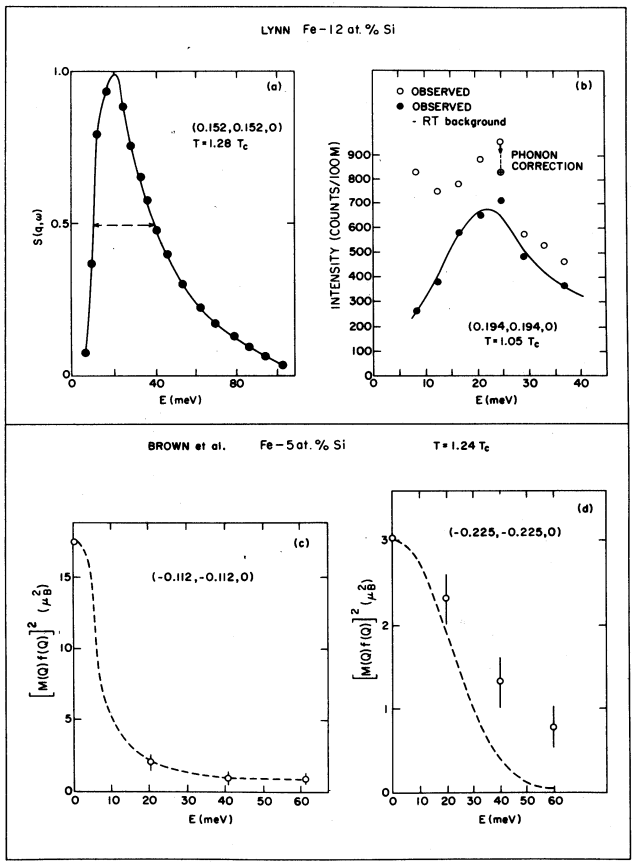

FIG. 8. Constant-q scans from two Fe(Si) alloys at reduced temperatures exceeding T_c. These scans have been obtained from (a) Lynn (Fig. 10), (b) Lynn (Fig. 2), and (c) and (d) Brown *et al.* (Fig. 3). Data denoted by closed circles in (b) result from the removal of a room-temperature (RT) background.

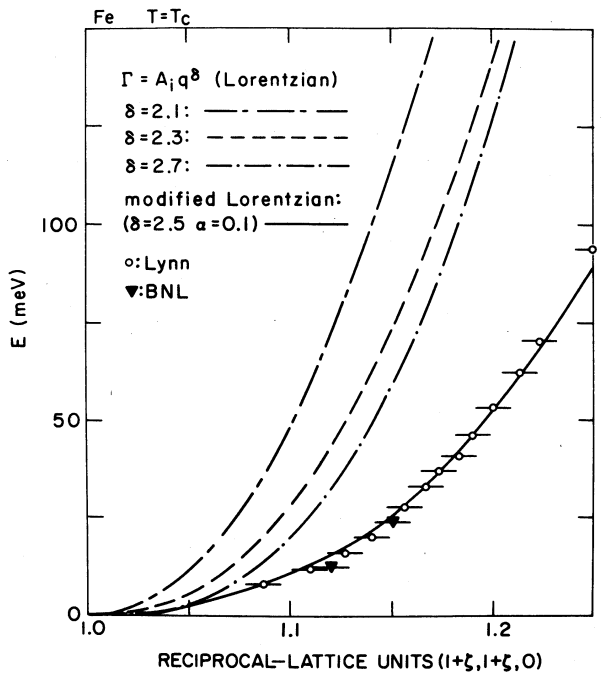

FIG. 9. Energy—versus—wave-vector calculations obtained from both the pure ($\alpha=0$) and modified ($\alpha=0.1$) Lorentzian forms of $S(q,\omega)$. Data denoted by open circles are copied from Ref. 3 (Fig. 2), while data denoted by solid triangles are our current results.

VI. DISCUSSION

There are two basic differences between our current polarized-beam study of both pure Fe and Fe—4 at.% Si and the previous unpolarized-beam reports[3,16] on Fe—12 at.% Si. The first difference is in the constant-q scans above T_c. No indication of a spin-wave-like peak is seen in our measurements (Figs. 3 and 4), as compared with the broad inelastic ridges observed in Figs. 8(a) and 8(b). As previously stated, we believe this difference is due to the problem of subtracting a correct background at small energy transfers when using unpolarized neutrons. The second difference is in the interpretation of the peaks observed above T_c in constant-energy scans. These peaks were previously interpreted[3] as spin waves yielding a spin-wave dispersion curve above T_c. The justification of this was in the conversion of $\Delta q/q$ to $\Delta E/E$ using the dispersion relation. We will illustrate that this conversion is not a justifiable one, and that both the constant-energy peaks and dispersion relation can be fairly well reproduced using a slightly modified form of the double Lorentzian given in Eqs. (2) and (8). A detailed description of this modification has recently been given by Böni *et al.*[26] In our discussion below we will utilize some of the highlights of Ref. 26, which includes the application of this modified scattering function to the paramagnetic scattering of iron. Such a modification is not unexpected and, in fact, has been discussed in some detail by Marshall and Lovesey[27] for the case of critical magnetic scattering at high temperatures and large q values.

Let us now write the paramagnetic scattering function, discussed in Sec. III, in a more general form:

$$S(q,\omega)=\frac{2}{3\pi}\frac{S(S+1)}{r_1^2}\frac{1}{\kappa_1^2+q^2}F(q,\omega)\frac{\omega/kT}{1-e^{-\omega/kT}} \tag{13}$$

where we now express the spectral weight function $F(q,\omega)$ as follows:

$$F(q,\omega)=\left[\frac{\Gamma}{\Gamma^2+\omega^2}\right]^{\epsilon(\omega)}, \tag{14}$$

with $\Gamma=Aq^{\delta}$. The constant-q scans in Secs. II and IV are well described using the simple Lorentzian form for $F(q,\omega)$ [$\epsilon(\omega)=1$]. However, there is some discrepancy with the peak position observed in constant-energy scans. In Fig. 9 we have plotted results for several model calculations for iron at $T=T_c$. This figure also includes measured data points from Ref. 3 as well as two constant-E

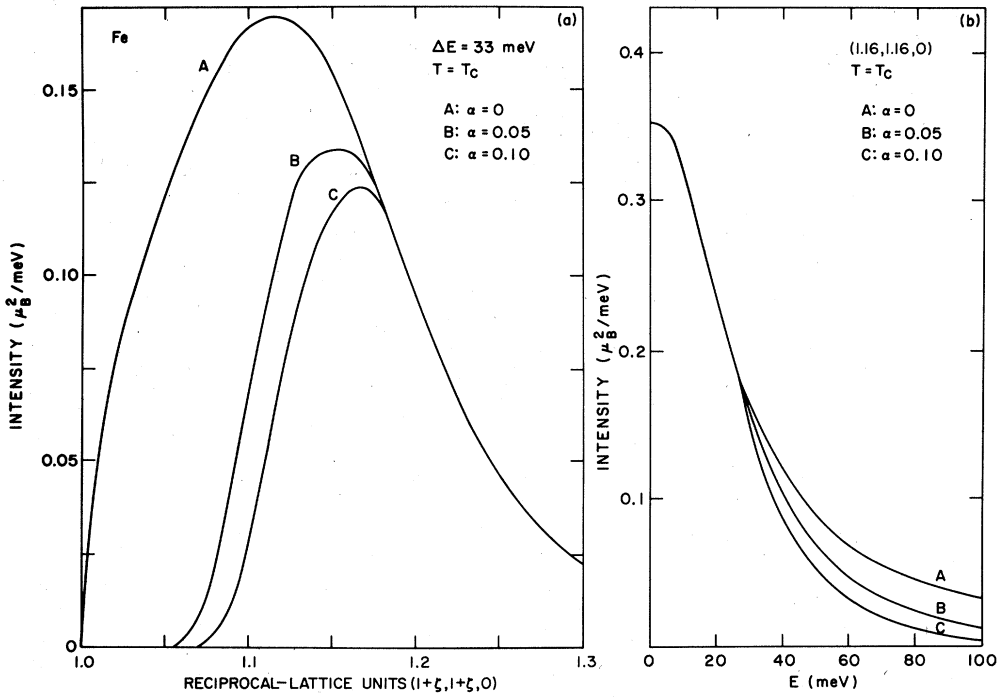

FIG. 10. (a) Constant-energy and (b) constant-q calculations obtained from the modified Lorentzian form of $S(q,\omega)$ for three different values of α. After Böni *et al.*

scans at $\Delta E=12$ and 24 meV obtained by us. Here, using Eqs. (13) and (14) with $\epsilon(\omega)=1$, we obtain

$$S(q,\omega)\propto\frac{1}{q^2}\frac{Aq^{\delta}}{(Aq^{\delta})^2+\omega^2} \tag{15}$$

This form of $S(q,\omega)$ always yields a constant-energy peak which is on the left-hand side of the data. Note that the peak position is not very sensitive to δ in the range $2.3<\delta<2.7$; however, when $\delta=2.0$ at $T=T_c$, the peak position is at $\zeta=0$ and yields constant-energy scans with intensities which monotonically decrease with increasing ζ. Lynn[16] has recently illustrated that use of a quadratic q dependence in $S(q,\omega)$ ($\delta=2.0$) yields a large discrepancy with his constant-E data, especially for large energy transfers at temperatures close to T_c. The reason for this disagreement is twofold: First, the proper value of the exponent δ must be used. This value has been shown to be 2.5. Second, the changeover of $F(q,\omega)$ from a pure Lorentzian must be made.

If a Gaussian form of $F(q,\omega)$ is used, the peak shape of $S(q,\omega)$ would be very asymmetric with a peak position on the right-hand side of the measured data and a peak intensity which is too high in value. We have, therefore, tried a modified form of $F(q,\omega)$ where $\epsilon(\omega)$ in Eq. (14) has the form

$$\epsilon(\omega)=\begin{cases}1, & |\omega|\le\Gamma\\ 1+\alpha[(|\omega|-\Gamma)/\Gamma], & |\omega|\ge\Gamma\end{cases}. \tag{16}$$

One new parameter has been introduced: α along with a fixed crossover point when $|\omega|=\Gamma$. For $\alpha>0$, $F(q,\omega)$ goes to zero faster than a pure Lorentzian ($\alpha=0$). By increasing α we can substantially shift the peak position in constant-energy scans to higher q values, whereas the line shapes in constant-q scans are only slightly modified in the tail. Note how well this form of $F(q,\omega)$ fits the measured data when $\delta=2.5$ and $\alpha=0.1$.

Let us now see how well we can reproduce the constant-energy peaks of Ref. 3. In Fig. 10(a) we have plotted a constant-energy peak for $E=33$ meV with $\alpha=0$, 0.05, and 0.10, and $\Gamma=Aq^{5/2}$ at $T=T_c$. Its position, width, and intensity agree much better with the measured data when $\alpha=0.1$ as compared to a pure Lorentzian ($\alpha=0$). The peak shape could be further improved by limiting $\epsilon(\omega)$ to a fixed value at some energy, i.e., at $E=5\Gamma$, $\epsilon=1.4$. Note that only the tail end of the constant-q scan in Fig. 10(b) is modified when α changes. Figure 11 shows intensity contours calculated with this modified double-Lorentzian form of $S(q,\omega)$ [Eqs. (13), (14), and (16)] with $\delta=2.5$ and $\alpha=0.1$. Once again, constant-energy peaks are seen in these contours, but a Lorentzian-type behavior, centered at zero energy, is still observed in constant-q slices. Note the difference between this figure and Fig. 1(b). The peaks in Fig. 11 are sharper and occur at larger q values for a given energy. The dispersion curve is given in Fig. 9.

Additional constant-energy—data comparisons are given in Figs. 12 and 13. Figure 12 compares this modified double-Lorentzian form of $S(q,\omega)$ with three constant-E scans obtained by Lynn using unpolarized

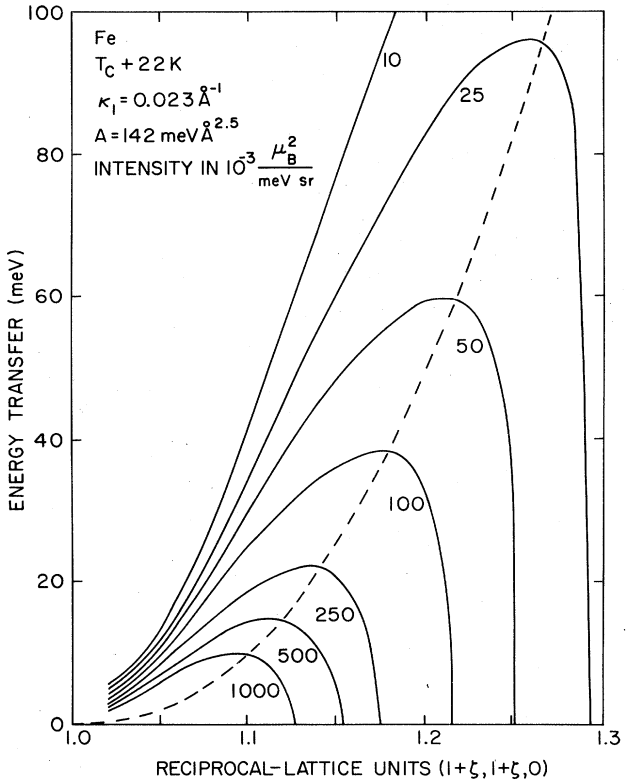

FIG. 11. Intensity counters calculated from the modified Lorentzian using $\alpha=0.1$ and $\delta=2.5$. Dashed line in this figure corresponds to the solid line in Fig. 9.

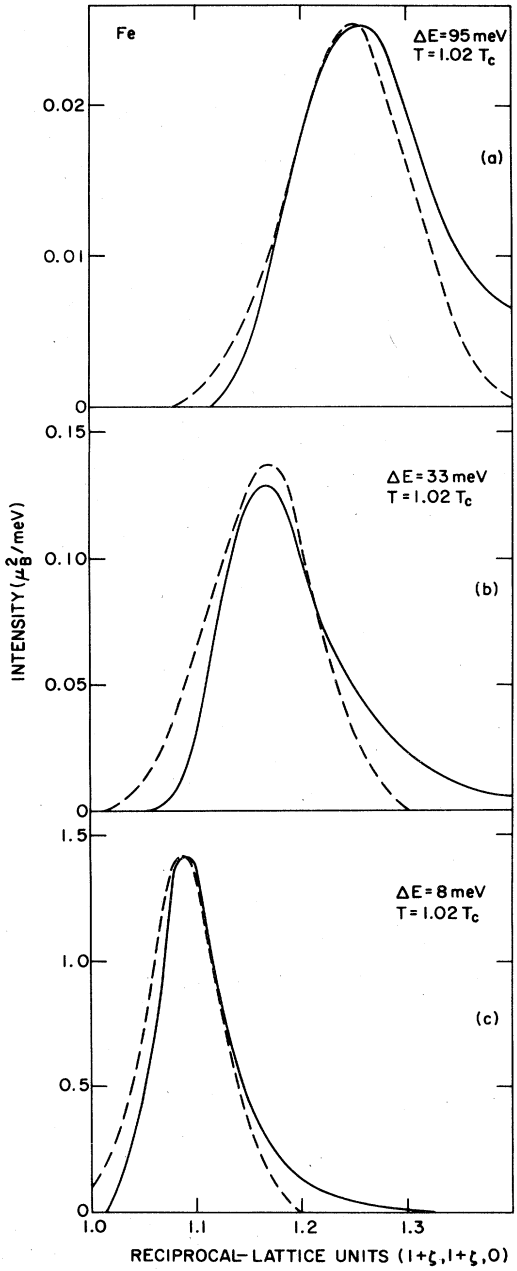

FIG. 12. Comparison of the modified Lorentzian calculation (solid lines) with three constant-energy measurements (dashed lines) obtained by Lynn (Ref. 16). Parameters used in the calculations are $\alpha=0.1$, $\delta=2.5$, and values in Table II at $T=1.02T_c$.

neutrons. The data in Fig. 13 are our constant-E measurements obtained using polarized neutrons and the HF−VF difference technique. The values of α and δ are the same as those in Fig. 11, while the parameters A and κ_1 are given in Table II. Data obtained at temperatures of $1.02T_c$ and $1.06T_c$ are shown with $E=24$ meV in Fig. 13. We conclude that the agreement in both Figs. 12 and 13 is quite satisfactory.

In Figs. 9—13 we have shown that the spin-wave concept is not a unique one in explaining the constant-energy results of Ref. 3. The conversion, therefore, of $\Delta q/q \rightarrow \Delta E/E$ is not justified since the spin-wave nature can never be uniquely determined via a constant-energy scan. Only constant-q scans can truly signify propagating excitations either above or below T_c. In our measurements on Fe, no constant-q spin waves have been observed in the q range covered above T_c.

Recently, some questions have been raised[28] concerning the validity of the double-Lorentzian form of $S(q,\omega)$ in conjunction with dynamical scaling. It was pointed out that both the peak positions and linewidths were different when comparing constant-energy data with the pure Lorentzian form of Eq. (13). These discrepancies are now removed using the simple changeover introduced in Eqs. (14) and (16). This is clearly evident in Figs. 10, 12, and 13.

It is important to look at the "constant-E" issue from the proper perspective. We estimate $S(Q,\omega)$, which is in units of μ_B^2 per meV, to be accurate to within 20% in the range up to 50 meV and $\zeta=0.15$. Of course, near $\Delta E=0$ we know the cross section with a higher accuracy. At the

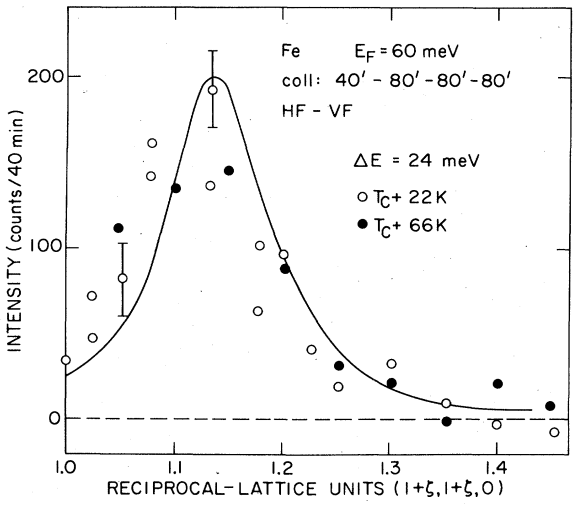

FIG. 13. Similar comparison as in Fig. 12, with our constant-energy data at $\Delta E = 24$ meV.

higher end of ω in $S(Q,\omega)$ (for example, at $\Delta E = 40$ meV and $\zeta > 0.2$), the cross section may be known to only 50% accuracy. If one studies $S(Q,\omega)$ in the same region only by constant-energy scans with $\Delta E \geq 8$ meV, but not including $\Delta E = 0$, then one covers less than 20% of the total cross section. As we have emphasized previously in Ni,[13] if one puts the cross sections into an absolute scale, then it is obvious that constant-E peaks represent marginal cross sections at the peak position of q.

Finally, we should point out that constant-E scans were dictated to us by a steep slope of the magnon dispersion curves in Fe and Ni. Once one is in the paramagnetic region (and if one has a polarized-beam instrument), then only constant-Q scans are necessary.

ACKNOWLEDGMENTS

The authors would like to thank D. M. Edwards, B. H. Grier, J. W. Lynn, C. F. Majkrzak, H. A. Mook, T. Moriya, B. S. Shastry, O. Steinsvoll, and Y. J. Uemura for helpful discussions and assistance during the course of these experiments. Work at Brookhaven National Laboratory was supported by the Division of Materials Sciences, U.S. Department of Energy, under Contract No. DE-AC02-76CH00016.

[1]See, for example, the recent review article by T. Moriya, J. Magn. Magn. Mater. **31-34**, 10 (1983).
[2]M. F. Collins, V. J. Minkiewicz, R. Nathans, L. Passell, and G. Shirane, Phys. Rev. **179**, 417 (1969).
[3]J. W. Lynn, Phys. Rev. B **11**, 2624 (1975).
[4]H. A. Mook, J. W. Lynn, and R. M. Nicklow, Phys. Rev. Lett. **30**, 556 (1973).
[5]J. W. Lynn and H. A. Mook, Phys. Rev. B **23**, 198 (1981).
[6]R. E. Prange and V. Korenman, Phys. Rev. B **19**, 4691 (1979); H. Capellmann, Z. Phys. B **34**, 29 (1979); J. B. Sokoloff, J. Phys. F **5**, 1946 (1975).
[7]B. S. Shastry, D. M. Edwards, and A. P. Young, J. Phys. C **14**, L665 (1981); D. M. Edwards, J. Magn. Magn. Mater. **15-18**, 262 (1980); B. S. Shastry (private communication).
[8]P. J. Brown, J. Déportes, D. Givord, and K. R. A. Ziebeck, J. Appl. Phys. **53**, 1973 (1982); **55**, 1881 (1984).
[9]P. J. Brown, H. Capellmann, J. Déportes, D. Givord, and K. R. A. Ziebeck, J. Magn. Magn. Mater. **30**, 243 (1982).
[10]P. J. Brown, H. Capellmann, J. Déportes, D. Givord, and K. R. A. Ziebeck, J. Magn. Magn. Mater. **30**, 335 (1983).
[11]D. M. Edwards, J. Magn. Magn. Mater. **36**, 213 (1983).
[12]O. Steinsvoll, C. F. Majkrzak, G. Shirane, and J. P. Wicksted, Phys. Rev. Lett. **51**, 300 (1983).
[13]O. Steinsvoll, C. F. Majkrzak, G. Shirane, and J. P. Wicksted, Phys. Rev. B **30**, 2377 (1984).
[14]J. P. Wicksted, G. Shirane, and O. Steinsvoll, Phys. Rev. B **29**, 488 (1984).
[15]J. P. Wicksted, G. Shirane, and O. Steinsvoll, J. Appl. Phys. **55**, 1893 (1984).
[16]J. W. Lynn, Phys. Rev. B **28**, 6550 (1983).
[17]V. J. Minkiewicz, M. F. Collins, R. Nathans, and G. Shirane, Phys. Rev. **182**, 624 (1969).
[18]Y. J. Uemura, G. Shirane, O. Steinsvoll, and J. P. Wicksted, Phys. Rev. Lett. **51**, 2322 (1983).
[19]G. Shirane, Y. J. Uemura, O. Steinsvoll, and J. P. Wicksted, J. Appl. Phys. **55**, 1887 (1984).
[20]Detailed discussions of this technique are given by K. R. A. Ziebeck and P. J. Brown [J. Phys. F **10**, 2015 (1980)] and R. M. Moon, T. Riste, and W. C. Koehler [Phys. Rev. **181**, 920 (1969)].
[21]A detailed discussion of this function is given in L. Passell, O. W. Dietrich, and J. Als-Nielsen, Phys. Rev. B **14**, 4897 (1976); P. Böni, B. H. Grier, G. Shirane, and Y. Ishikawa (unpublished).
[22]R. Résibois and C. Piette, Phys. Rev. Lett. **24**, 514 (1970).
[23]G. Parette and R. Kahn, J. Phys. (Paris) **32**, 447 (1971).
[24]This function has been shown to break down for $q < 0.02$ Å^{-1} by F. Mezei, Phys. Rev. Lett. **49**, 1096 (1982).
[25]S. Boronkay and M. F. Collins, Int. J. Magn. **4**, 205 (1973).
[26]P. Böni, G. Shirane, and J. P. Wicksted (unpublished).
[27]W. Marshall and S. W. Lovesey, *Thermal Neutron Scattering* (Oxford University Press, London, 1971), p. 493.
[28]J. W. Lynn, Phys. Rev. Lett. **52**, 775 (1984).